

Cucurbit[8]Uril Driven Upconversion Near-Infrared Delayed Fluorescence for Targeted Cell Imaging

Shuangqi Song, Xuan Zhao, Hengzhi Zhang, Lihua Wang, and Yu Liu*

Pure organic upconversion systems have opened new possibilities for deep-tissue bioimaging based on efficient two or three-photon excitation. Herein, a pure organic room-temperature phosphorescence (RTP) upconversion supramolecular assembly is reported that exhibits near-infrared (NIR) delayed fluorescence by upconverted excitation at 940 nm. This system is constructed by co-assembling cucurbit[8]uril (CB[8])-confined indole-bridged xanthene derivative (CyBr) with the complex of CB[8] encapsulated two sulfonated bromophenylpyridinium (PySO3 ⊂CB[8]), guided by β -cyclodextrin-grafted hyaluronic acid (HACD). First, the spatial confinement of CB[8] 10-fold enhances the fluorescence of CyBr. Subsequently, as the tumor-targeting agent, HACD realizes cascade fluorescence enhancement, boosting the quantum yield (QY) of CyBr by 22 times. Moreover, the cavities of β -CDs in HACD provide assembly sites for multivalent interactions with the sulfonic acid group of PySO₃ ⊂CB[8], achieving highly efficient phosphorescence resonance energy transfer (PERT) with an efficiency of 84.49%. This leads to NIR delayed fluorescence at 710 nm with a lifetime of 99.16 µs. Notably, this system exhibits exceptional upconversion capability under 940 nm three-photon excitation, enabling targeted A549 cancer cell imaging with deep-tissue penetration and long-lived NIR emission for low-background detection.

1. Introduction

Supramolecular upconversion systems with unique long-wavelength excitation characteristics and highly efficient anti-Stokes luminescence have demonstrated significant application potential in deep-tissue bioimaging, [1,2] precision theranostics, [3,4] anti-counterfeiting encryption, [5,6] and optoelectronic devices. [7,8] Among existing strategies, lanthanide-based upconversion systems utilizing the characteristic 4f–4f transitions have been well-developed. [9-10] Despite effective emission and photostability, biological applications still face numerous challenges, including the requirement for sophisticated surface coating to ensure colloidal stability and reduce potential

S. Song, X. Zhao, H. Zhang, L. Wang, Y. Liu College of Chemistry State Key Laboratory of Elemento-Organic Chemistry Nankai University Tianjin 300071, P. R. China E-mail: yuliu@nankai.edu.cn

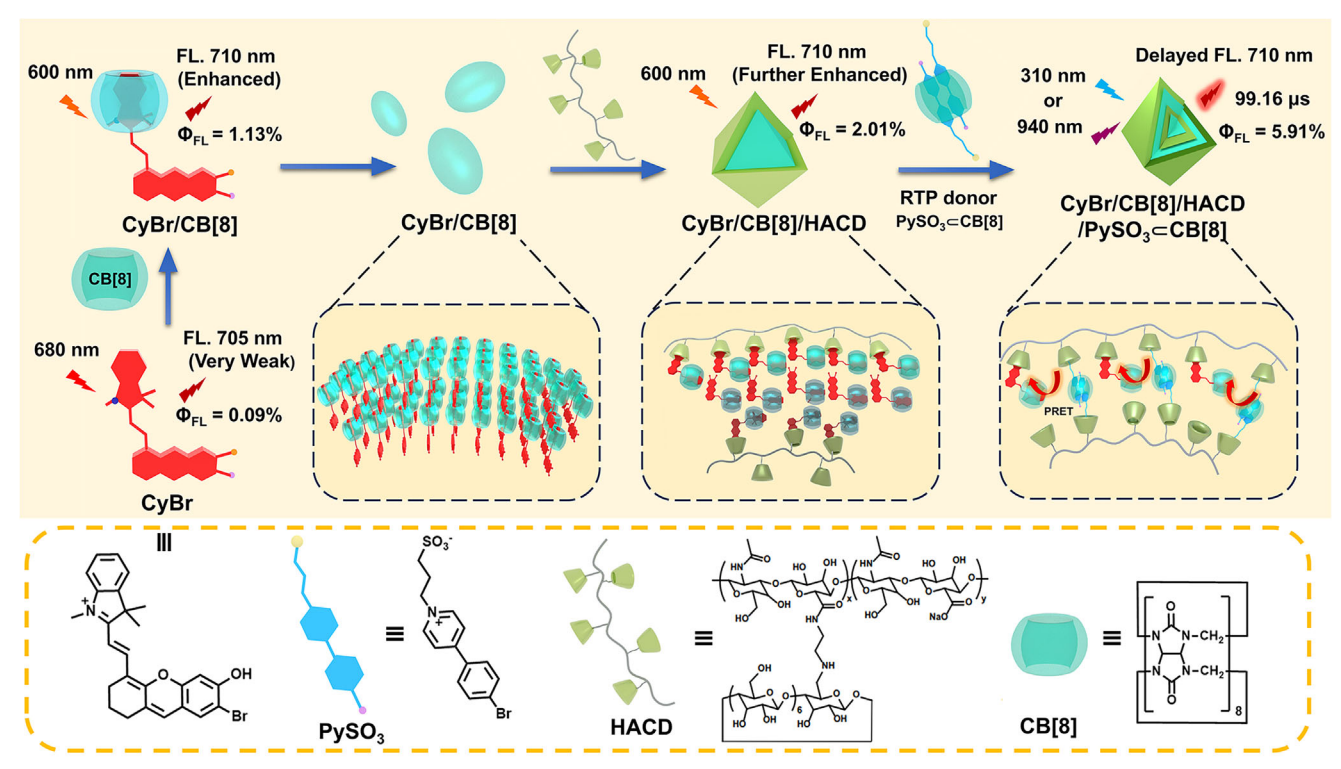
The ORCID identification number(s) for the author(s) of this article can be found under https://doi.org/10.1002/smll.202507202

DOI: 10.1002/smll.202507202

cytotoxicity.[11-14] Meanwhile, small-molecule probes based on multiphoton absorption have been extensively explored for biomedical applications.[15,16] By extending π -conjugation and enhancing intramolecular charge transfer (ICT) effects, these designed molecules effectively reduce the energy gap between ground and excited states to realize upconversion emission. For instance, Tang et al. reported a donor- π -acceptor structured molecule that leveraged intense ICT to enable two-photon excited near-infrared (NIR) imaging and photodynamic therapy, achieving 940 µm-depth brain imaging and precise treatment of small-size glioblastoma, thus advancing fluorescence-guided therapy.[17] Recently, macrocycle-based supramolecular strategies have emerged as a powerful approach for constructing pure organic upconversion materials.[18,19] The hydrophobic cavities of macrocyclic hosts can encapsulate poorly soluble guest molecules, not only improving their biocompatibility but also inducing and enhancing luminescent behaviors through spatial confinement. Furthermore, such

supramolecular confinement promotes charge transfer (CT) effects, enabling efficient two-/three-photon absorption processes.[20-22] For example, Stoddart and coworkers designed and synthesized a series of novel tetracationic macrocycles that encapsulated 5,15-diphenylporphyrin to achieve triplet-triplet annihilation upconversion luminescence through precise host-guest interactions.^[23] Our research group has also reported a NIR excited and emitting organic room-temperature phosphorescence (RTP) material based on cucurbit[8]uril (CB[8]) confinement, where unimolecular self-folding of the guests induced strong between donor and acceptor moieties, resulting in two-photon absorption and tunable luminescence extending to 800 nm in the NIR region. Further nanoassembly significantly enhanced the phosphorescence intensity while preserving the two-photon properties, enabling successful bioimaging applications.^[24] Recently, Ma et.al. also reported CB[8]-confined a series of bromophenylpyridine derivatives to induce the molecular folding, which exhibited the unique temperature-dependent upconversed RTP property.[25] However, CB[8] has driven not only the enhancement of fluorescence but also the upconversion-achieved cascade assembly to give NIR delayed fluorescence has been rarely reported to the best of our knowledge.

16136289, 0, Downloaded from https://onlinelibrary.wiley.com/doi/10.1002/sml.10.02507202 by Nankai University, Wiley Online Library on [24/10/2025]. See the Terms and Conditions (https://onlinelibrary.wiley.com/rems-and-conditions) on Wiley Online Library for rules of use; OA articles are governed by the applicable Creative Commons License



Scheme 1. Hypothetical assembly mechanism for cucurbit[8]uril driven upconversion cascade assembly for NIR delayed fluorescence targeted cell imaging.

Herein, we report the CB[8] driven pure organic upconversion supramolecular assembly, in which not only the CB[8]-confined indole-bridged xanthene derivative (CyBr) realized the fluorescence-enhancement but also the β -cyclodextrinmodified hyaluronic acid (HACD) cascade assembled with CyBr/CB[8] and sulfonated bromophenylpyridinium-CB[8] complex (PySO3CCB[8]) to achieve phosphorescence energy transfer (PRET) (Scheme 1). CB[8] encapsulated CyBr exhibited significantly enhanced fluorescence intensity at 710 nm. The introduction of HACD enabled multifunctional integration, where the further confined microenvironment progressively enhanced the fluorescence quantum yield (QY) of CyBr from an initial 0.09 to 2.01% through the cascade effect. Meanwhile, the cyclodextrin cavities provided co-assembly sites for incorporating the phosphorescent donor (PySO₃ CCB[8]), enabling the efficient PRET process with an efficiency of 84.49%, which ultimately generated NIR delayed fluorescence at 710 nm with a lifetime of 99.16 µs and a QY of 5.91%. Notably, while maintaining the inherent cancer cell-targeting capability of hyaluronic acid (HA), the system has excellent upconversion luminescence performance under 940 nm three-photon excitation, which successfully achieved targeted imaging of A549 tumor cells.

2. Results and Discussion

The CyBr was synthesized according to the previously reported procedures,[26] and the chemical structure was characterized by nuclear magnetic resonance spectroscopy (NMR) and highresolution mass spectrometry (HRMS) (Figures \$1-\$3, Supporting Information). The bonding behavior of the CB[8] and guest was first studied through UV-vis spectroscopy experiments. When CB[8] was added gradually, the maximum absorption of CyBr was blueshifted from 750 to 600 nm (Figure 1a), and the color of the solution was changed from light blue to dark blue, which may be due to the encapsulation of CB[8] cavities, resulting in preventing the aggregation of the guest molecules themselves. Subsequently, the related bonding constant (K_a) was measured to be 5.06×10^7 m⁻¹ by nonlinear least-squares analysis of the absorbance intensity changes of CyBr at 550 nm (Figure S8, Supporting Information). The 1:1 stoichiometry ratio for CyBr/CB[8] was verified through Job's plot experiment (Figure S9, Supporting Information) and HRMS, where the strong m/z peak at 1792.473 could be attributed to [CyBr+CB[8]-I]+ (Figure \$10, Supporting Information). Furthermore, the strong host-guest interaction was also confirmed by ¹H NMR titration experiment. In the presence of CB[8], the protons in the indole groups showed a significant upfield shift, suggesting that the indole moieties were deeply encapsulated within the cavity of CB[8] (Figure S11, Supporting Information). Furthermore, the 2D ROSEY experiment also corroborated the binding mode of CyBr/CB[8] (Figure S12, Supporting Information). The comprehensive experimental results above indicated that the positively charged indole salt portion of CyBr was encapsulated by CB[8] to form a 1:1 complex driven by the ion-dipole interactions and hydrophobic interactions. In order to study the luminescent behavior of macrocyclic confinement, the photoluminescence (PL) spectra have been performed to show that the guest molecule exhibited a very weak emission peak at 705 nm, and with the addition of CB[8], the fluorescence intensity increased significantly, and the QY was enhanced from 0.09% to 1.13% (Figure 1b). CyBr is a typical

www.small-journal.com

16136289, 0, Downloaded from https://onlinelibrary.wiley.com/doi/10.1002/sml1.202507202 by Nankai University, Wiley Online Library on [2410/2025]. See the Terms and Conditions (https://onlinelibrary.wiley.com/rems-and-conditions) on Wiley Online Library for rules of use; OA articles are governed by the applicable Creative Commons License

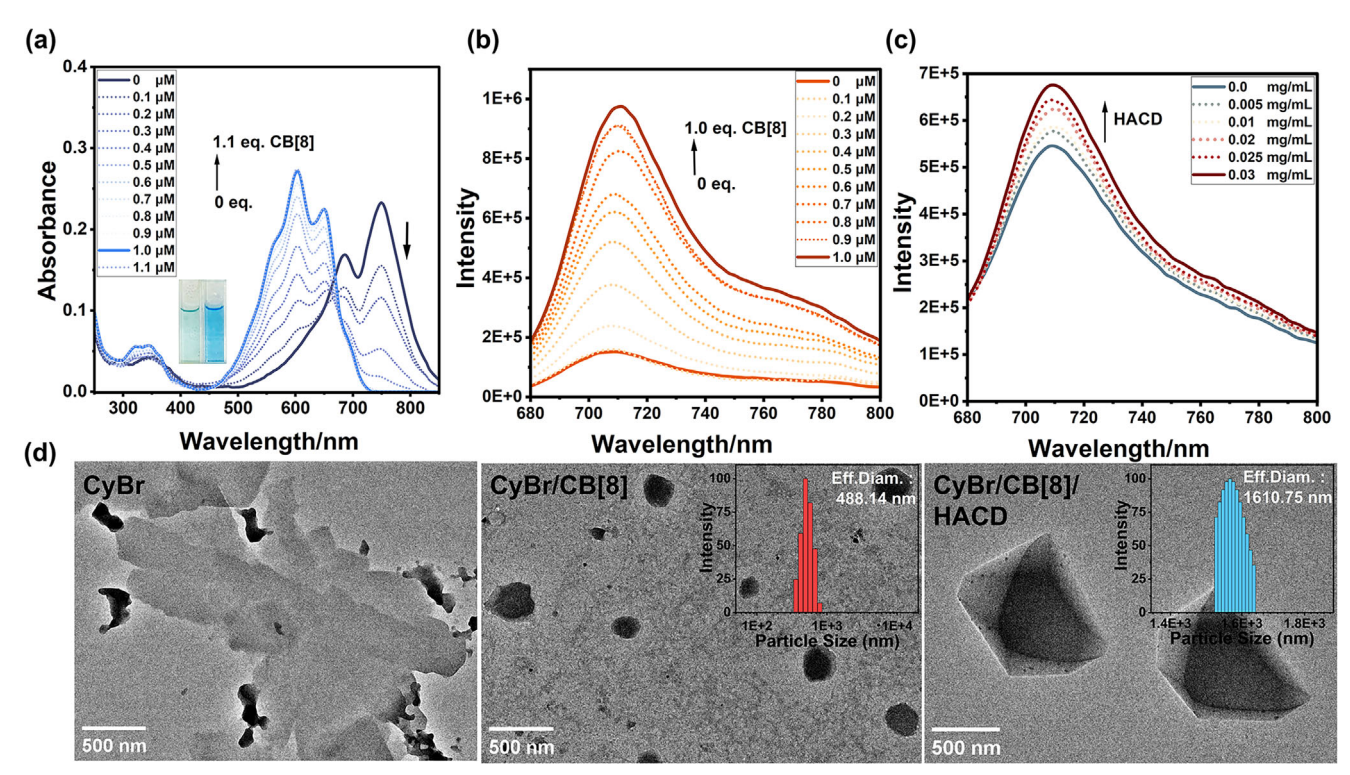


Figure 1. a) UV–vis absorption spectra changes of CyBr upon the addition of 0–1.1 eq. CB[8] in H₂O at 298 K ([CyBr] = 10 μm, CB[8] = 0–11 μm). PL emission spectral changes of b) CyBr upon addition of 0–1.0 eq. CB[8] in H₂O at 298 K and c) CyBr/CB[8] upon addition of 0–0.03 mg mL⁻¹ HACD in H₂O at 298 K. ([CyBr] = 10 μm, [CB[8]] = 0–10 μm, λ_{ex} = 600 nm). d) TEM images of CyBr, CyBr/CB[8], and CyBr/CB[8]/HACD (inset: DLS data of CyBr/CB[8] and CyBr/CB[8]/HACD, [CyBr] = [CB[8]] = 10 μm; [HACD] = 0.03 mg mL⁻¹).

molecule that can undergo ICT from donor xanthines to acceptor indole salts, and by investigating its UV-vis and PL spectra in solvents of different polarity (Figure S13a,b, Supporting Information), it can be observed that CyBr has obvious solvent dependence, with significant fluorescence quenching in highly polar solvents (water). The emission intensity was recovered in highviscosity solutions (glycerol) and at low temperatures (Figure S13c,d, Supporting Information), which showed that CyBr was the typical twisted intramolecular charge transfer (TICT) characteristic molecule. These results suggested that the rigid cavity of macrocyclic CB[8] effectively restricted the molecular motion of CyBr, which facilitated the ICT process to improve the luminescence in an aqueous solution. In addition, in comparison with the PL spectra of CyBr/CB[7] (Figure S14, Supporting Information), CB[8] with a larger cavity was able to encapsulate the guest molecule more deeply, which can enhance the luminescence performance of the guest molecule more significantly.

The HACD possesses a large number of negative charges that can cascade assembly with the positively charged CyBr and CB[8] complex. Therefore, HACD (Figure S7, Supporting Information), as the cancer cell-targeted agent, was introduced for secondary assembly with CyBr/CB[8]. As demonstrated in Figure 1c, with the gradual addition of HACD, the fluorescence intensity of CyBr/CB[8] at 710 nm was further enhanced. This intensity reached a state of equilibrium at a concentration of HACD of 0.03 mg mL $^{-1}$. Furthermore, the QY was increased from 1.13% to 2.01% by virtue of the cascade assembly of HACD. Additionally, two other negatively charged molecules, HA and

sulfonated calix[4]arene (SC4A), were selected to investigate the influence of secondary assembly on the photophysical properties of the supramolecular assembly. After the addition of HA, no significant change in fluorescence was observed, whereas the introduction of SC4A significantly suppressed the emission intensity (Figure \$15, Supporting Information). This phenomenon may be attributed to the fact that HACD can not only co-assemble through electrostatic interactions, but the cavities of cyclodextrins also partially encapsulate the xanthene ring of CyBr. In contrast, the hydrophobic alkyl chains of SC4A induced stronger π - π stacking of CyBr, leading to significant fluorescence quenching. Based on these, it can be concluded that the coassembly with HACD provided the optimal supramolecular environment, which is conducive to further fluorescence enhancement. Through the investigation of the spectral characteristics of the CyBr/HACD direct assembly system (Figure S16, Supporting Information), we observed a noticeable decrease in fluorescence intensity. This quenching phenomenon may be attributed to two primary factors: 1) the relatively weak binding affinity of the cyclodextrin cavity for CyBr, and 2) the strong electrostatic interaction by HA unexpectedly promoted molecular stacking of CyBr. The above results exhibited the crucial importance of cascade assembly strategies.

To comprehensively characterize the topological morphology of the progress of CyBr/CB[8]/HACD, we further utilized a set of complementary analytical methods, including transmission electron microscopy (TEM), scanning electron microscopy (SEM), dynamic light scattering (DLS), and zeta potential

16136289, 0, Downloaded from https://onlinelibrary.wiley.com/doi/10.1002/sml.10.02507202 by Nankai University, Wiley Online Library on [24/10/2025]. See the Terms and Conditions (https://onlinelibrary.wiley.com/rems-and-conditions) on Wiley Online Library for rules of use; OA articles are governed by the applicable Creative Commons License

www.small-journal.com

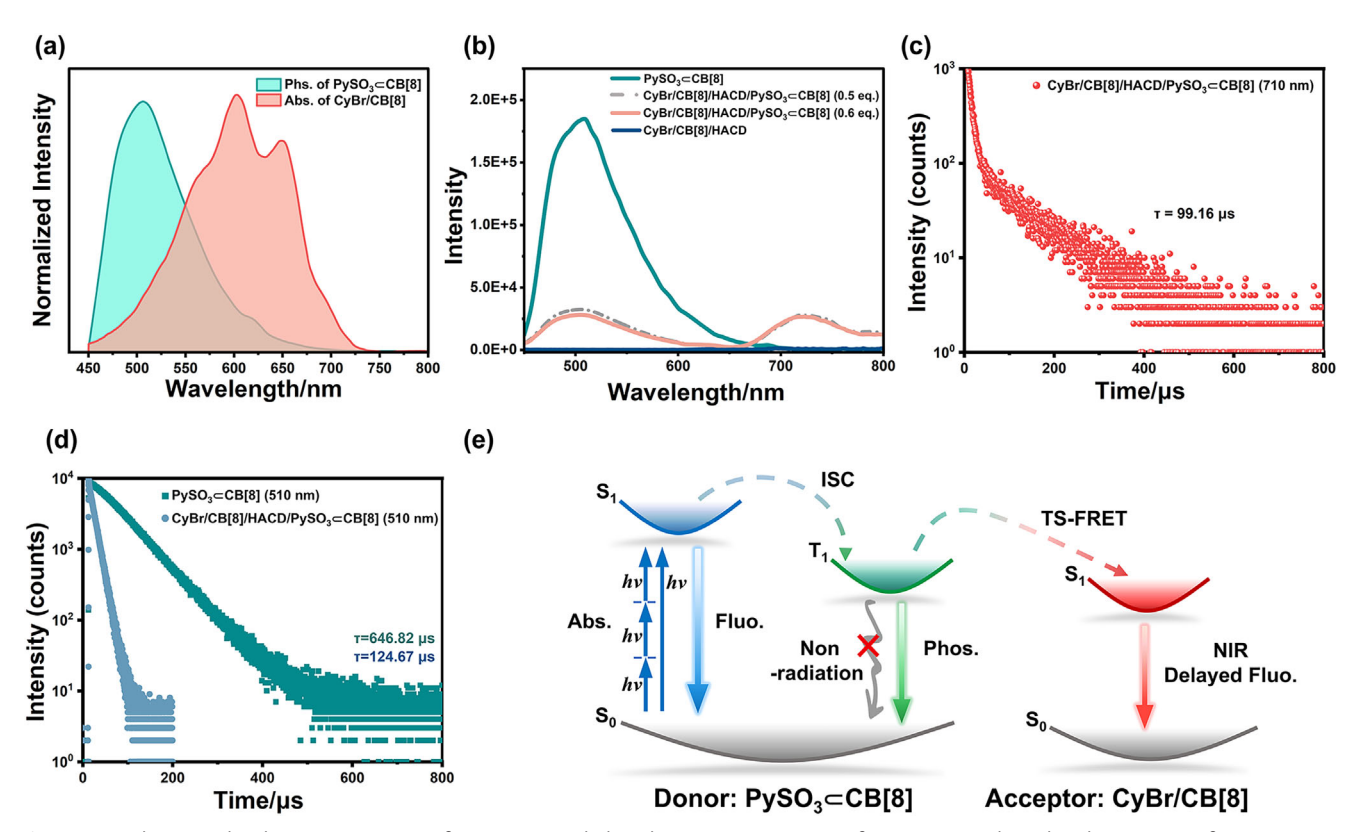


Figure 2. a) The normalized UV–vis spectrum of CyBr/CB[8] and phosphorescence spectrum of PySO₃ \subset CB[8]. b) Delayed PL spectra of PySO₃ \subset CB[8], CyBr/CB[8]/HACD/PySO₃ \subset CB[8] (0.5 and 0.6 eq. PySO₃ \subset CB[8]) and CyBr/CB[8]/HACD ([CyBr] = 10 μM, [CB[8]] = 10 μM, [HACD] = 0.03 mg mL⁻¹, λ_{ex} = 310 nm). c) The delayed fluorescence lifetime of CyBr/CB[8]/HACD/PySO₃ \subset CB[8] at 710 nm ([CyBr] = 10 μM, [CB[8]] = 10 μM, [HACD] = 0.03 mg mL⁻¹, [PySO₃ \subset CB[8]] = 5 μM, λ_{ex} = 310 nm). d) Phosphorescence lifetime of PySO₃ \subset CB[8] and CyBr/CB[8]/HACD/PySO₃ \subset CB[8] (0.5 eq. PySO₃ \subset CB[8]) at 510 nm (λ_{ex} = 310 nm). e) Proposed mechanism illustrating the supramolecular energy transfer pathway (ISC = inter-system crossing, TS-FRET = Triplet to singlet Förster resonance energy transfer).

measurements. TEM images showed that CyBr self-stacked into irregular flakes, which were encapsulated by CB[8] to form ellipsoidal nanoparticles with a diameter of ≈450 nm, and after secondary assembly with HACD, the ellipsoidal nanoparticles transformed into polyhedral particles with diameters ranging from 1.5 to 2 µm (Figure 1d). The DLS results indicated that CyBr/CB[8] had an average diameter of 488 nm, while CvBr/CB[8]/HACD displayed an average diameter of 1611 nm. The corresponding morphologies were also observed in SEM (Figure \$17, Supporting Information). Furthermore, Tyndall effect experiments also confirmed that CyBr/CB[8]/HACD aggregated to larger assemblies than CyBr/CB[8] (Figure S18a, Supporting Information). The average zeta potential of CyBr/CB[8] was +13.82 mV, and after co-assembly with negatively charged HACD, the average zeta potential of CyBr/CB[8]/HACD was -26.74 mV (Figure S18b,c, Supporting Information). Taking all these into consideration, the supramolecular cascade assembly was successfully constructed, driven by synergistic hydrophobic and electrostatic interactions.

Benefiting from the exceptional NIR luminescence of the ternary supramolecular assembly CyBr/CB[8]/HACD, it is expected to further introduce the phosphorescence donors to achieve PRET for the generation of long-lived NIR delayed fluorescence. Within the CyBr/CB[8]/HACD, the sulfonated bromophenylpyridinium derivative (PySO₃) and CB[8] complex served as the energy-transfer donor components. Gated PL

spectra revealed that with the incremental addition of CB[8], the emission intensity of PySO₃ at 510 nm was progressively induced and significantly enhanced (Figure \$20, Supporting Information). Upon nitrogen purging of the PySO₃CCB[8] solution, the emission intensity was markedly increased (Figure S21a, Supporting Information), accompanied by the lifetime was extended from 0.647 to 1.513 ms (Figure S21b, Supporting Information). These findings conclusively assign the long-lived emission at 510 nm to phosphorescence. Job's plot analysis and UV-vis spectroscopy confirmed a 2:1 binding stoichiometry between PySO3 and CB[8], with the K_a of 1.07 \times 10⁸ M^{-2} (Figure S22, Supporting Information). ¹H NMR titration spectroscopy demonstrated that upon the addition of CB[8], the aromatic protons of the bromophenylpyridine moiety in PySO₃ exhibited a pronounced upfield shift (Figure S23, Supporting Information), and the system reached equilibrium at 0.5 equivalents of CB[8], demonstrating the encapsulation of two bromophenylpyridine units of PySO₃ within a single CB[8] cavity. For the PySO₃/ β -CD system, the protons on the alkyl chain in PySO3 shifted downfield, confirming the inclusion of the sulfonated alkyl chain by β -CD. Moreover, the introduction of β -CD in PySO₃CCB[8] still induced a downfield shift of the alkyl protons, further evidencing that the sulfonated alkyl chain of PySO₃ \subset CB[8] was included by β -CD (Figure \$24, Supporting Information). To validate the proposed assembly model in Scheme 1 and address the structure of the

16136289, 0, Downloaded from https://onlinelibrary.wiley.com/doi/10.1002/sml1202507202 by Nankai University, Wiley Online Library on [24102025]. See the Terms and Conditions (https://onlinelibrary.wiley.com/rems-and-conditions) on Wiley Online Library for rules of use; OA articles are governed by the applicable Creative Commons Licensen

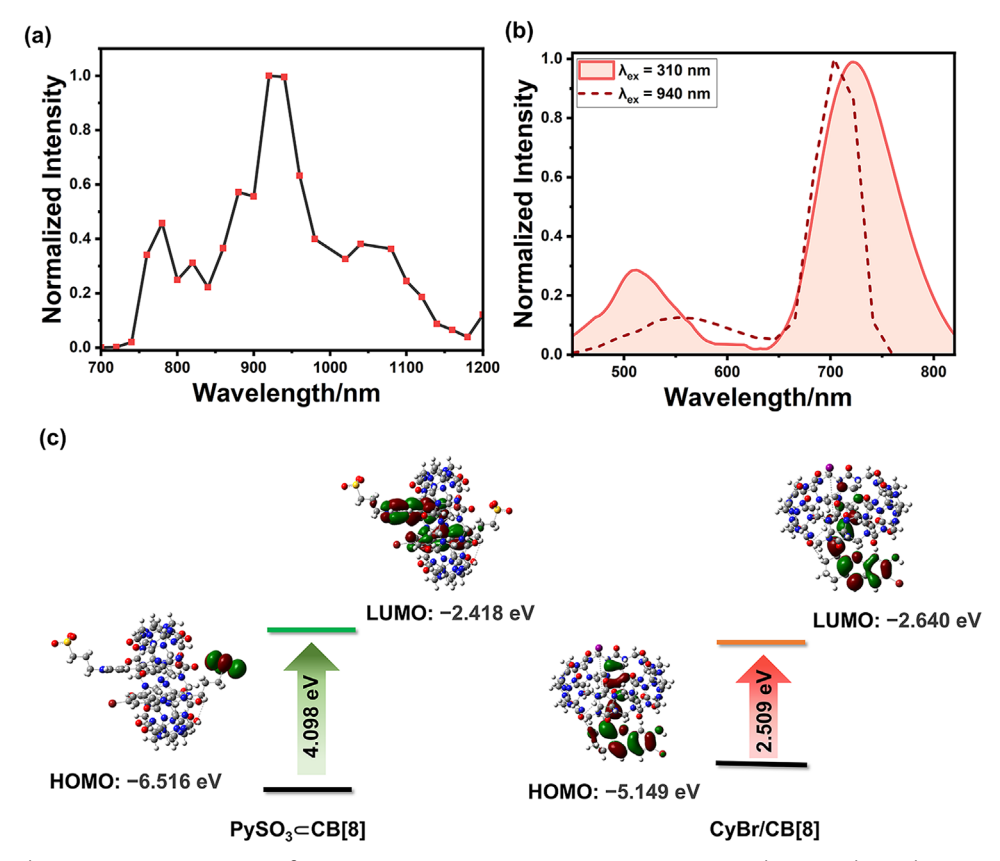


Figure 3. a) Three-photon excitation spectrum of CyBr/CB[8]/HACD/PySO₃ \subset CB[8] in an aqueous solution under ambition conditions. ([CyBr] = [CB[8]] = 10 μm, [HACD] = 0.03 mg mL⁻¹, [PySO₃ \subset CB[8]] = 5 μm) b) Three-photon and single-photon emission spectra of assembly CyBr/CB[8]/HACD/PySO₃ \subset CB[8] excited with different wavelengths in an aqueous solution under ambition conditions. ([CyBr] = [CB[8]] = 10 μm, [HACD] = 0.03 mg mL⁻¹, [PySO₃ \subset CB[8]] = 5 μm). c) The calculated spatial distributions of HOMO and LUMO for PySO₃ \subset CB[8] and CyBr/CB[8].

final complex, further characterization was conducted. TEM and DLS results revealed that the addition of PySO₃ CB[8] led to the formation of assemblies with smaller and more uniform morphology, exhibiting an average diameter of 672.71 nm (Figure \$19, Supporting Information). We speculate that PySO₃⊂CB[8] acts as a crosslinker, with its host-guest interaction with β -CD facilitating the synergistic co-assembly of CyBr/CB[8]/HACD into a more compact and ordered architecture. This assembly process was further corroborated by an enhanced Tyndall effect (Figure \$18a, Supporting Information) and a significant increase in the positive zeta potential of the assemblies (Figure S18b,c, Supporting Information). In summary, we successfully constructed a supramolecular assembly with NIR delayed fluorescence. Compared to the CyBr/CB[8]/HACD, its smaller and more uniform size overcomes the potential obstacles of large nanoparticles in biological applications, laying a foundation for cell imaging and future in vivo applications.

As evidenced by **Figure 2a**, the phosphorescence emission band of $PySO_3 \subset CB[8]$ exhibited substantial spectral overlap with the absorption profile of CyBr/CB[8]/HACD, demonstrating the feasibility of $PySO_3 \subset CB[8]$ to serve as an energy donor for the PRET. Upon introduction of $PySO_3 \subset CB[8]$ into the CyBr/CB[8]/HACD assembly, gated PL spectroscopy showed a new long-lived emission peak at 710 nm, which was absent in the pristine CyBr/CB[8]/HACD assembly (Figure 2b), and

the system reached emission equilibrium upon the addition of 0.5 equivalents of PySO₃ ⊂ CB[8]. Time-resolved PL decay analysis further demonstrated a 99.16 µs lifetime at 710 nm for the CyBr/CB[8]/HACD/PySO₃CCB[8] system (Figure 2c). Concurrently, the phosphorescence intensity of PySO3 CCB[8] was significantly reduced after energy transfer compared to the original, with the lifetime also decreasing from 646.82 to 124.67 µs (Figure 2d). Based on the change in phosphorescence intensity at 510 nm, it was concluded that the TS-FRET efficiency (E)[27] was 84.49%, which was basically consistent with the efficiency calculated based on the change in lifetime (E = 80.73%). The CyBr/CB[8]/HACD system exhibited a photoluminescence QY of 5.91%. Collectively, the CB[8]-confined PySO₃ exhibited efficient phosphorescence emission (QY = 11.87%), and through the incorporation of PySO₃⊂CB[8] into CyBr/CB[8]/HACD, the spatial distance between the energy donor (PySO₃CCB[8]) and singletstate acceptor (CyBr/CB[8]) was significantly reduced, thereby effectively promoting the TS-FRET process, ultimately achieving long-lived NIR emission at 710 nm in an aqueous solution. The proposed working mechanism of this supramolecular cascade energy transfer system was illustrated in Figure 2e.

Recently, pure organic upconversion phosphorescent materials have been widely used in biomedical applications due to their nonlinear optical properties and biocompatibility. The NIR multiphoton excitation mode has deeper tissue penetration, lower

16136289, 0, Downloaded from https://onlinelibrary.wiely.com/doi/10.1002/sml1.202507202 by Nankai University, Wiley Online Library on [24/10/2025]. See the Terms and Conditions (thtps://onlinelibrary.wiley.com/terms-and-conditions) on Wiley Online Library for rules of use; OA articles are governed by the applicable Creative Commons Licenses

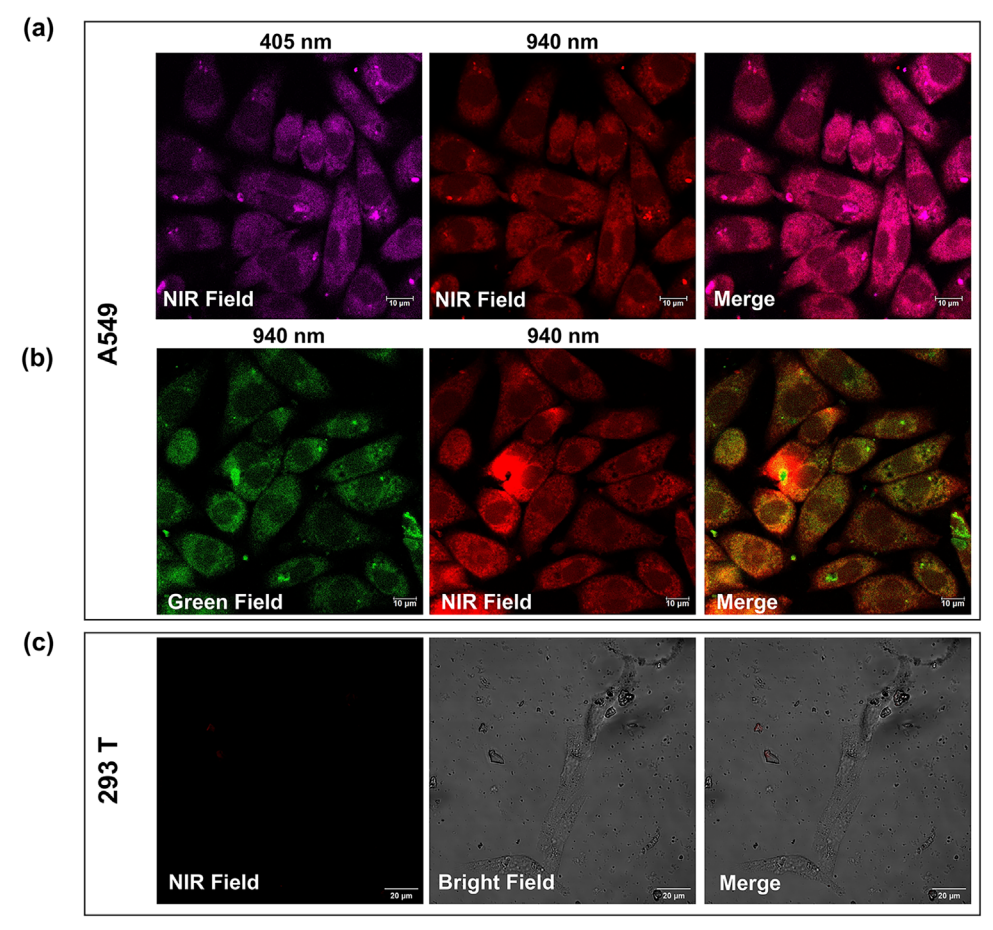


Figure 4. Cellular imaging of CyBr/CB[8]/HACD/PySO₃ CCB[8] supramolecular assembly. a) A549 cancer cells imaged under 405 nm single-photon (left), 940 nm three-photon (middle), and merged (right). b) Three-photon microscopy (940 nm excitation) of A549 cancer cells showing emission in the green (480–530 nm, component PySO₃ CB[8] phosphorescence) and red (680–780 nm, NIR delayed fluorescence) channels with merged overlay. c) Control imaging of 293T normal cells under 405 nm excitation (red channel: 650–800 nm).

phototoxicity, and weaker background interference, and combined with the long-lived emission of phosphorescence, it can significantly improve the imaging signal-to-noise ratio.[28,29] Therefore, we first investigated the three-photon absorption properties of PySO₃ ⊂CB[8]. As anticipated, femtosecond laser pulse measurements showed that D displayed an excitation wavelength range of 750-1100 nm (Figure S25a, Supporting Information). The fluorescence spectrum of PySO₃⊂CB[8] under 940 nm excitation showed emission peaks at 550 nm, similar to those observed under single-photon excitation at 310 nm (Figure S25b, Supporting Information). In control experiments, the guest molecule PySO3 did not exhibit significant three-photon excitation peaks in the 700-1200 nm range, and no detectable fluorescence under three-photon imaging, which contrasted sharply with the bright fluorescence observed from PySO₃ nanoparticles under single-photon excitation (Figure S26, Supporting Information). These results demonstrated the importance of the confinement of CB[8] for upconversion phosphorescence. Subsequently, we investigated the feasibility of energy transfer under the three-photon excitation. The cascade assembly CyBr/CB[8]/HACD/PySO₃⊂CB[8] also displayed distinct threephoton absorption characteristics, with a particularly prominent excitation peak at 940 nm (Figure 3a). Notably, when excited by 940 nm femtosecond laser pulses, the assembly maintained the NIR fluorescence emission at 700-710 nm (Figure 3b), which also overlapped well with the fluorescence profile obtained under conventional 310 nm excitation, confirming the preservation of TS-FRET under three-photon excitation conditions. Subsequently, we testified to the mechanism of three-photon excitation energy transfer by theoretical calculations. As illustrated in Figure 3c, the HOMO electron density of donor PySO₃⊂CB[8] is primarily localized on the sulfonic acid group of the PySO₃, while the LUMO density is concentrated on the bromophenylpyridinium moiety. This apparent spatially separated CT characteristic enhanced three-photon absorption efficiency and provided orbital coupling channels for energy transfer.[30,31] The HOMO-LUMO energy gap of 4.098 eV closely matched the total energy required for three-photon excitation at 940 nm. Besides, the acceptor assembly CyBr/CB[8] exhibited a smaller bandgap with closely aligned LUMO levels to the donor, thus facilitating efficient energy transfer.

Given the combined advantages of NIR-delayed fluorescence emission, three-photon absorption properties, and HACD-conferred cancer cell targeting specificity, the

___small

CyBr/CB[8]/HACD/PySO₃CCB[8] supramolecular assemblies were expected to be applied as upconverted NIR-targeted bioimaging probes. A cytotoxicity evaluation was first conducted using two representative cells, human non-small cell lung cancer cells (A549) and human embryonic kidney cells (293T). Quantitative analysis of CCK-8 showed that cell viability remained above 85% at concentrations up to 12 μm, which confirmed the system had very low cytotoxicity and met the requirements for biomedical applications (Figure S27, Supporting Information). The CyBr/CB[8]/HACD/PySO₃CCB[8] supramolecular nanocomplexes were incubated with 293T and A549 for 12 h to allow cellular internalization before upconversion multiphoton imaging. As shown in Figure 4a, distinct NIR fluorescence signals were detected under both 405 nm singlephoton and 940 nm three-photon excitation modes. Notably, 940 nm three-photon excitation provided excellent resolution by reducing cellular scattering and autofluorescence while maintaining good cellular penetration. Furthermore, under 940 nm excitation, the imaging system simultaneously captured green phosphorescence emission from component PySO₃⊂CB[8] and PRET-induced NIR delayed fluorescence (Figure 4b). While A549 cells displayed intense dual-channel emissions, 293T cells only exhibited the residual background signal (Figure 4c). The observed differential cellular uptake may be attributed to preferential internalization of CyBr/CB[8]/HACD/PySO₃⊂CB[8] in cancer cells, likely mediated through HA receptors (e.g., CD44) that are characteristically overexpressed in malignant cell lines. Subcellular distribution of the assembly was subsequently investigated through organelle colocalization experiments. When co-incubated with MitoTracker Green (mitochondria) and LysoTracker Green (lysosomes), confocal imaging demonstrated substantial overlap between the NIR emission from CyBr/CB[8]/HACD/PySO3CCB[8] and the green fluorescence of MitoTracker Green (Figure S28, Supporting Information), with a high Pearson correlation coefficient of 0.94 (Figure S29, Supporting Information), whereas the Pearson correlation coefficient with the green fluorescence of LysoTracker Green was only 0.29 (Figure \$30, Supporting Information), confirming predominant mitochondrial localization. The above experimental results established that CyBr/CB[8]/HACD/PySO3CCB[8] supramolecular cascade assembly can be used as the material for upconversion NIR-delayed fluorescence cellular imaging.

3. Conclusion

In summary, a supramolecular cascade assembly with three-photon NIR-delayed fluorescence at 710 nm with a lifetime of 99.16 μs was fabricated from CyBr, CB[8], HACD, and PySO₃CCB[8], which not only realized the enhancement of fluorescence through the cascade confinement but also achieved pure organic upconversion NIR emission to successfully apply in three-photon high-contrast targeted cellular imaging. Through the spatial confinement of the cavities of CB[8], the fluorescence intensity of the CyBr was significantly enhanced. The subsequent secondary assembly with HACD further extended the NIR emission and introduced precise hyaluronic acid-CD44 targeting functionality. Capitalizing on the achieved fluorescence enhancement, incorporation of the PySO₃CCB[8] as the phosphorescent donor enabled efficient PRET with an efficiency of 84.49%,

generating NIR-delayed fluorescence (710 nm) with a 99.16 μs lifetime, and the QY was increased from 0.09% to 5.91% in an aqueous solution. Notably, under 940 nm three-photon excitation, the assembly exhibited exceptional upconversion capability for targeted A549 cancer cell imaging, which provides a new approach to achieve pure organic upconversion cascade energy transfer to NIR delayed fluorescence for targeted cell imaging.

4. Experimental Section

Statistical Analysis: Data from cell viability assays were reported as mean \pm SD (n=3). Spectroscopic measurements were repeated at least three times. Co-localization analysis (Pearson's coefficient) was performed using ImageJ with the Colocalization Finder plugin. Formal statistical testing was not applicable to the core photophysical data.

Detailed experimental procedures and characterization data are provided in the Supporting Information.

Supporting Information

Supporting Information is available from the Wiley Online Library or from the author.

Acknowledgements

The authors thank the National Natural Science Foundation of China (NNSFC, Grant Nos. 22131008), China Fundamental Research Funds for the Central Universities for financial support. The image acquisition was supported by the Biological Imaging and Analysis Laboratory, Medical and Health Analysis Center, Peking University, especially Jing Wu.

Conflict of Interest

The authors declare no conflict of interest.

Data Availability Statement

The data that support the findings of this study are available from the corresponding author upon reasonable request.

Keywords

cell imaging, delayed fluorescence, macrocyclic cucurbit[n]uril, supramolecular assembly, upconversion

Received: June 17, 2025 Revised: October 7, 2025 Published online: 16136289, 0, Downloaded from https://onlinelibrary.wiley.com/doi/10.1002/sml1.202507202 by Nankai University, Wiley Online Library on [2410/2025]. See the Terms and Conditions (https://onlinelibrary.wiley.com/rems-and-conditions) on Wiley Online Library for rules of use; OA articles are governed by the applicable Creative Commons License

- [1] X.-C. Duan, G.-Q. Zhang, S.-L. Ji, Y. Zhang, J. Li, H. Ou,Z. Gao, G. Feng, D. Ding, Angew. Chem., Int. Ed. 2022, 61,202116174.
- [2] C. Ouyang, Y. Li, T W. Rees, X. Liao, J. Jia, Yu Chen, X. Zhang, L. Ji, H. Chao, Angew. Chem., Int. Ed. 2021, 60, 4150.
- [3] Y.-Y. Liu, X.-F. Meng, W.-B. Bu, Coord. Chem. Rev. 2019, 379, 82.

16136829, 0, Downloaded from https://onlinelibrary.wiley.com/doi/10.1002/smll.202507202 by Nankai University, Wiley Online Library on [24/10/2025]. See the Terms and Conditions

(https://onlinelibrary.wiley.com/terms-and-conditions) on Wiley Online Library for rules of

use; OA

articles are governed by the applicable Creative Commons License

- [4] D. B. L. Teh, A. Bansal, C. Chai, T. B. Toh, R. A. J. Tucker, G. G. L. Gammad, Y. Yeo, Z. Lei, X. Zheng, F. Yang, J S. Ho, N. Bolem, B. C. Wu, M. K. Gnanasammandhan, L. Hooi, G. S. Dawe, C. Libedinsky, W-Yi Ong, B. Halliwell, E. K.-H. Chow, K.-L. Lim, Y. Zhang, B K. Kennedy, Adv. Mater. 2020, 32, 2001459.
- [5] K. Jiang, L. Zhang, J. Lu, C. Xu, C. Cai, H. Lin, Angew. Chem., Int. Ed. 2016, 55, 7231.
- [6] B.-W. Yang, X.-F. Yang, Y.-H. Shi, X. Jin, T. Li, M. Liu, P. Duan, Angew. Chem., Int. Ed. 2025, 64, 202417223.
- [7] S. Geng, H. Li, Z. Lv, Y. Zhai, B. Tian, Y. Luo, Ye Zhou, Su-T Han, Adv. Mater. 2025, 2419678.
- [8] C. Gao, W. W. H. Wong, Z. Qin, S.-C. Lo, E. B. Namdas, H. Dong, W. Hu, Adv. Mater. 2021, 33, 2100704.
- [9] S. Mohanty, A. M. Kaczmarek, Chem. Soc. Rev. 2022, 51, 6893.
- [10] X. Chen, X. Zhang, Y. Zhao, Chem. Soc. Rev. 2025, 54, 152.
- [11] Z.-C. Luo, Z.-G. Yi, X.-G. Liu, Acc. Chem. Res. 2023, 56, 425.
- [12] H. Ling, D. Guan, R. Wen, J. Hu, Y. Zhang, F. Zhao, Y. Zhang, Q. Liu, Small 2024, 20, 2309035.
- [13] A. Pilch-Wrobel, A. M. Kotulska, S. Lahtinen, T. Soukka, A. Bednarkiewicz, Small 2022, 18, 2200464.
- [14] H.-H. Li, W. Sheng, S. A. Haruna, M. M. Hassan, Q.-S. Chen, Compr. Rev. Food Sci. Food Saf. 2023, 22, 3732.
- [15] Y.-L. Yang, C. Cen, L.-J. Kan, Q. Zhao, Z. Huang, S. Li, *Interdiscip. Mater.* 2025, 4, 109.
- [16] L.-L. Wu, J.-H. Liu, P. Li, B. Tang, T. D. James, Chem. Soc. Rev. 2021, 50, 702
- [17] Z. Xu, X. Li, Z. Yang, Z. Zhang, Y. Zhang, M. Fan, Y. Zeng, M. Kang, Y. Shen, D. Wang, G. Xu, B. Z. Tang, Adv. Mater. 2025, 37, 2413164.
- [18] M.-J. Gu, X.-N. Han, W.-C. Guo, Y. Han, C.-F. Chen, Angew. Chem., Int. Ed. 2023, 62, 202305214.

- [19] Yu Wang, H. Wu, P. Li, Su Chen, L O. Jones, M A. Mosquera, L. Zhang, K. Cai, H. Chen, X.-Y. Chen, C L. Stern, M R. Wasielewski, M A. Ratner, G C. Schatz, J. F Stoddart, *Nat. Commun.* 2020, 11, 4633.
- [20] X. Zhao, X.-L. Zhou, W.-W. Xing, Y. Liu, Chem. Commun. 2023, 59, 11516.
- [21] X.-L. Zhou, X. Bai, X.-J. Zhang, J. Wu, Y. Liu, Adv. Opt. Mater. 2024, 12. 2301550.
- [22] Y. Li, Z. Wu, Z. Huang, C. Yin, He Tian, X. Ma, Natl. Sci. Rev. 2024, 12. nwae383.
- [23] I. Roy, A. Garci, Y. Beldjoudi, R M. Young, D J. Pe, M T. Nguyen, P. J. Das, M R. Wasielewski, J. F Stoddart, J. Am. Chem. Soc. 2020, 142, 16600.
- [24] X.-K. Ma, X.-L. Zhou, J. Wu, F.-F. Shen, Y. Liu, Adv. Sci. 2022, 9, 2201182.
- [25] Y. Li, Z. Huang, A. Shao, Z. Wu, Z. He, He Tian, X. Ma, Chem. Sci. 2025. 16, 6290.
- [26] L. Yuan, W. Lin, S. Zhao, W. Gao, B. Chen, L. He, S. Zhu, J. Am. Chem. Soc. 2012, 134, 13510.
- [27] M. Huo, X.-Y. Dai, Y. Liu, Small 2022, 18, 2104514.
- [28] J. Li, X. Li, G. Wang, X. Wang, M. Wu, J. Liu, K. Zhang, Nat. Commun. 2023, 14, 1987.
- [29] H. Chen, B. Qi, T. Moore, D C. Colvin, T. Crawford, J C. Gore, F. Alexis, O. T Mefford, J N. Anker, *Small* **2014**, *10*, 160.
- [30] Y. Li, S. Liu, H. Ni, H. Zhang, H. Zhang, C. Chuah, C. Ma, K. S. Wong, J W. Y. Lam, R T. K. Kwok, J. Qian, X. Lu, B. Z. Tang, Angew. Chem., Int. Ed. 2020, 59, 12822.
- [31] Y.-J. Hong, W.-H. Geng, T. Zhang, G. Gong, C. Li, C. Zheng, F. Liu, J. Qian, M. Chen, B. Z. Tang, Angew. Chem., Int. Ed. 2022, 61, 202209590.